Organic Electronics Hot Paper

How to cite: *Angew. Chem. Int. Ed.* **2022,** *61,* e202210939
International Edition: doi.org/10.1002/anie.202210939
German Edition: doi.org/10.1002/ange.202210939

Vibration-Assisted Charge Transport through Positively Charged Dimer Junctions

Xin Zhu[+], Boyu Wang[+], Wan Xiong[+], Shuyao Zhou, Kai Qu, Jing-Tao Lü, Hongliang Chen,* Chuancheng Jia,* and Xuefeng Guo**

Abstract: Intermolecular charge transport plays a vital role in the fields of electronics, as well as biochemical systems. Here, we design supramolecular dimer junctions and investigate the effects of charge state and energy level alignment on charge transport under nanoconfinement. Incoherent tunneling caused by thermally-induced vibrations is enhanced in positively charged systems. The transition between coherent and incoherent tunneling is associated with specific molecular vibration modes. Positively charged systems with smaller torsional barriers and vibrational frequencies result in lower transition temperatures. Multiple thermal effects have a great impact on the conductance in the off-resonant tunneling, while thermally-induced vibron-assisted tunneling contributes more to the transport in the resonant tunneling. These investigations offer a deep mechanism understanding of intermolecular charge transport and facilitate the development of practical functional molecular devices.

Introduction

Intermolecular charge transport plays a key role in chemistry,[1] biology,[2] and organic electronics.[3] In particular, in the field of organic electronics, such as organic field-effect transistors,[4] organic light-emitting diodes,[5] organic photovoltaics,[6] and organic thermoelectrics,[7] the charge state and orbital characteristics of molecules have a great impact on intermolecular interactions that are intimately associated with the device performance.[8] From the view of a single molecule, a better understanding of the factors affecting charge transport through adjacent molecules is beneficial for the development of organic electronics.[9] To this end, single-molecule junction (SMJ) techniques provide useful tools for investigating intermolecular charge transport.[10] Dynamic single-molecule junctions,[11] such as scanning tunneling microscope break junction and mechanically controlled break junction, have been used to investigate the charge transport mechanisms of π-stacked dimers. The intermolecular stacking conformations of the dimer could be manipulated by stretching the electrodes,[10c,12] during which various physical properties, such as quantum interference effect,[12b,c] have been observed. Further efforts should be made to systematically investigate the intermolecular transport mechanisms, especially the influence of structural factors on charge transport behaviors. Indeed, the molecular charge state, as a significant feature, enables to control the mechanism of single-molecule devices, such as rectifiers,[13] transistors,[14] and switches.[15]

Supramolecular assembly facilitates the formation of stable dimers with well-defined molecular geometries and separation distances, enabling the fabrication of reliable dimer junctions for single-molecule electrical measurements, which is beneficial for understanding the mechanism of intermolecular charge transport.[16] For instance, host–guest interactions, using cucurbit[8]uril (CB[8]) as a macrocyclic host, have been applied to obtain dynamic single-molecule junctions.[16d,17] In this work, using graphene-based static molecular junctions as a stable measurement platform,[18] we

[*] X. Zhu,[+] B. Wang,[+] Prof. C. Jia, Prof. X. Guo
Center of Single-Molecule Sciences, Institute of Modern Optics, Tianjin Key Laboratory of Micro-scale Optical Information Science and Technology, Frontiers Science Center for New Organic Matter, College of Electronic Information and Optical Engineering, Nankai University
38 Tongyan Road, Jinnan District, Tianjin 300350 (P. R. China)
E-mail: jiacc@nankai.edu.cn
guoxf@pku.edu.cn

X. Zhu,[+] S. Zhou, Prof. C. Jia, Prof. X. Guo
Beijing National Laboratory for Molecular Sciences, National Biomedical Imaging Center, College of Chemistry and Molecular Engineering, Peking University
292 Chengfu Road, Haidian District, Beijing 100871 (P. R. China)

W. Xiong,[+] Prof. J.-T. Lü
School of Physics, Institute for Quantum Science and Engineering and Wuhan National High Magnetic Field Center, Huazhong University of Science and Technology
Wuhan 430074 (P. R. China)
E-mail: jtlu@hust.edu.cn

K. Qu, Prof. H. Chen
Stoddart Institute of Molecular Science, Department of Chemistry, Zhejiang University
Hangzhou 310021 (P. R. China)
E-mail: hongliang.chen@zju.edu.cn

K. Qu, Prof. H. Chen
ZJU-Hangzhou Global Scientific and Technological Innovation Center
Hangzhou 311215 (P. R. China)

[+] These authors contributed equally to this work.

construct dimer-based single-molecule junctions (SMJs) containing positively charged units through supramolecular host–guest interaction. Based on temperature-dependent measurements, the intermolecular charge transport mechanism of dimers is explored in terms of charge state and energy level under nanoconfinement.

Results and Discussion

To investigate the relationship between supramolecular structural characteristics and intermolecular charge transport properties in dimers, three types of dimers with different charge states and molecular frontier orbital energies have been designed to construct supramolecular dimer junctions (Figure 1a). As shown in Figure 1b, both monomer 1 (M1) and monomer 3 (M3) contain a positively charged pyridinium and differ in the degrees of conjugation, that is, M1 has a fully conjugated anthracene unit while M3 shows a broken conjugation with two pyridine units separated by two methylene units. Monomer 2 (M2) is a control molecule with a highly conjugated anthracene backbone and a neutral phenyl group. The details relating to the molecular synthesis and the formation of the host–guest complexes are provided in the Methods section and the Supporting Information (Scheme S1 and Figures S1–S4). To predict the effect of charge state and conjugation on the energy level alignments, theoretical analysis has been carried out. The calculated electrostatic potential maps (Figure 1b) demonstrate that the entire M1 has a positive electrostatic potential. However, the positive charge tends to be dispersed on the positively charged pyridinium unit instead of the neutral region of anthracene. This phenomenon suggests that the electrostatic potential distribution of positively charged molecules relative to neutral molecules is not uniform, which might lead to the corresponding dimers with distinct characteristics. In addition, the structural characteristics associated with the charge state and conjugation degree make stacked ways of dimers different, further resulting in diverse energy level alignments of dimers. Compared with the guest molecules, the calculated energy level alignments show that the HOMO–LUMO gaps of the corresponding dimers (Figure 1c) reduce to some extent, which are consistent with the results of UV/Vis spectra (Figure S4). The theoretical results demonstrate that molecular engineering is an efficient tool to tune the molecular energy level alignments, providing a basis for exploring the effects of molecular characteristics on intermolecular charge transport properties in dimers.

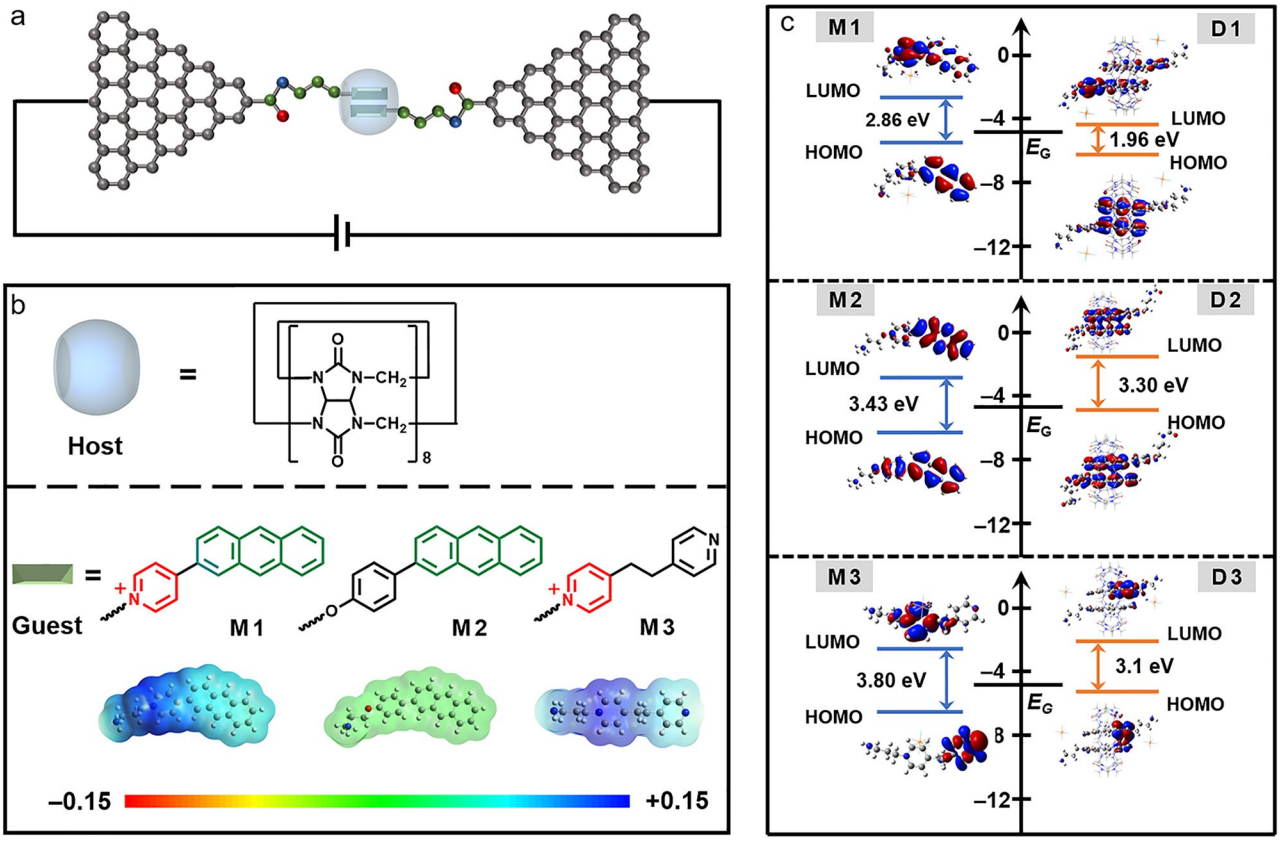

Figure 1. Supramolecular dimer-based SMJs and molecular characteristics. a) Illustration showing the device geometry, where the supramolecular complex is covalently connected to graphene electrodes. b) Structural formula of host and guest molecules, and corresponding calculated electrostatic potential maps. c) Calculated molecular energy levels and related molecular orbital diagrams (LUMO and HOMO) of monomers (left) and dimers (right). E_G is the work function of graphene.

In this work, cucurbit[8]uril (CB[8]) is chosen as the host molecule, and two guest molecules can be encapsulated inside the host cavity through a controllable π-stacked way to form a host–guest complex.[19] After assemblies of CB[8] with guest molecules (M1, M2, and M3), the terminal amine groups on guest molecules are covalently bonded to carboxyl groups at the end of graphene nanogap electrodes,[20] resulting in the formation of static SMJs, namely SMJ-1, SMJ-2, and SMJ-3, respectively. It is worth mentioning that three methylene (–CH_2–) groups are incorporated into the molecular backbone of monomers, which weakens molecule-electrode coupling and reduces the interference of the electrodes on inherent states of central dimers.[21] The detailed preparation steps for the dimer junctions are given in the Supporting Information (Figures S5 and S6). The successful preparation of single-molecule junctions can be determined by comparing the current–voltage (*I–V*) curves before and after connection of targeted supramolecular complexes, which show "nA"-level currents (Figure S7). The well-designed dimer systems provide the foundation for studying the effects of charge and conjugation on intermolecular charge transport.

To explore the structure–property relationship of supramolecular dimers, temperature-dependent measurements were performed, which help to understand the inherent transport mechanism from the change of molecular conductance with temperature.[22] Temperature-dependent *I–V* curves, with temperature scanning from 10 K to 300 K under a bias range of ±1 V, were performed under a high-vacuum condition in the dark (Figures 2a–c and S8–S12). As the temperature increased from 10 to 300 K, a large enhancement of current at high temperatures and a slow increase at low temperatures were observed for all three SMJs. The conductance of SMJ-1 with the positive charges shows a greater variation from 10 to 300 K, an increase about 6-fold at 1 V, while that of the neutral SMJ-2 increases about 3-fold (Figures 2a–c).

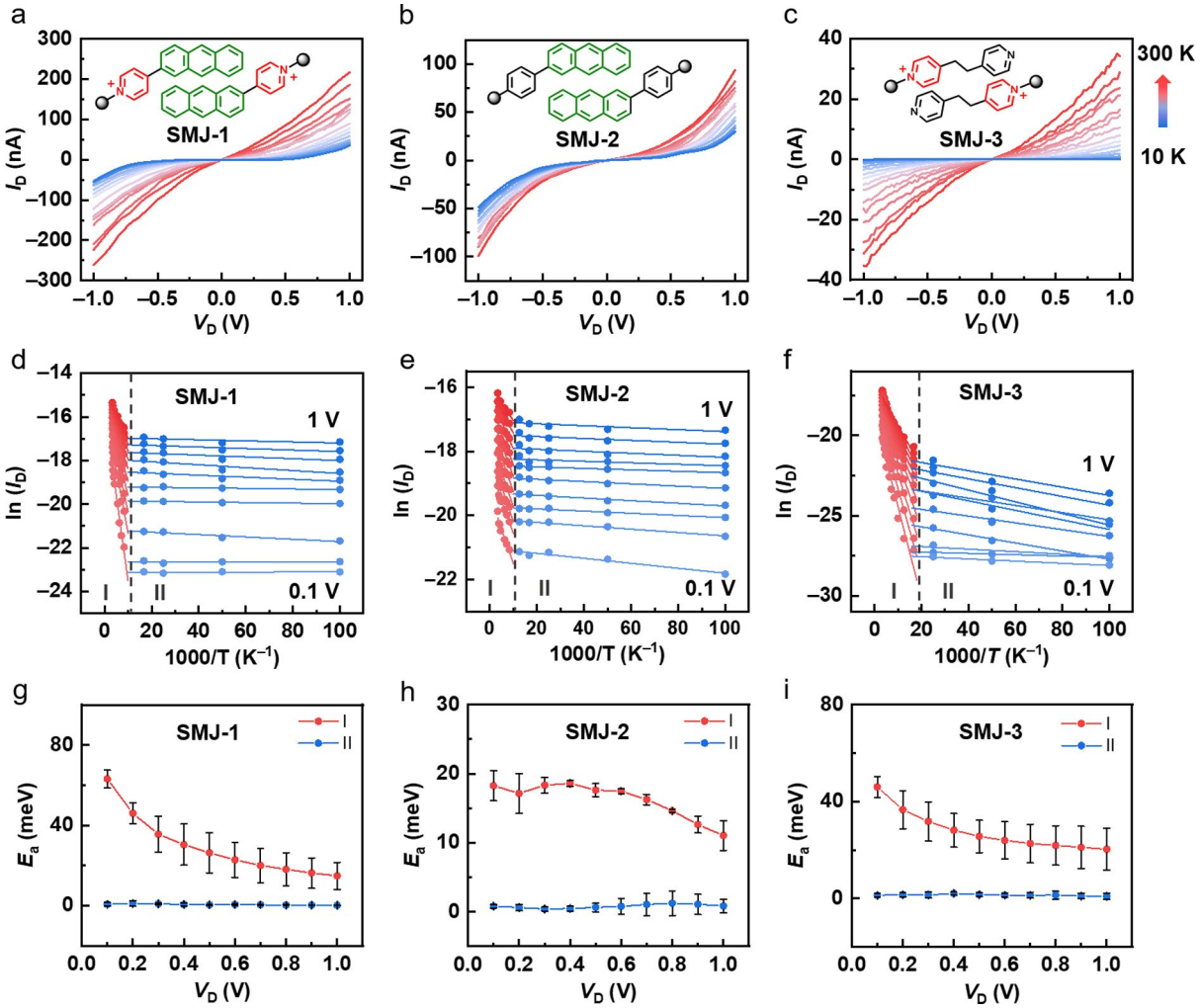

Figure 2. Temperature-dependent charge transport characteristics. *I–V* curves at different temperatures for a) SMJ-1, b) SMJ-2, and c) SMJ-3. Arrhenius plots of ln (I_D) versus 1/T for d) SMJ-1, e) SMJ-2, and f) SMJ-3 at different positive bias voltages with bias steps of 0.1 V. Bias-dependent activation energies for g) SMJ-1, h) SMJ-2, and i) SMJ-3, where I and II represent the high and low temperature regions, respectively. Error bars are obtained from three devices in each case.

An in-depth analysis of the *I–V* characteristics was conducted to gain a fundamental understanding of the intermolecular charge transport mechanism. Arrhenius plots of three representative SMJs obtained from the *I–V* curves show two regions, i.e., (i) a high temperature-dependent and (ii) low temperature-independent transport regimes (Figures 2d–f). In the high temperature region, according to thermally activated formulas:[22a,23]

$$\Delta E = -(1/k_B)[d(\ln I)/d(1/T)] \quad (1)$$

where k_B is the Boltzmann constant and T is the temperature, the activation energy (ΔE) of the temperature-dependent regime are extracted as ≈70 meV, ≈20 meV and ≈50 meV for SMJ-1, SMJ-2, and SMJ-3 at 0.1 V, respectively. This phenomenon suggests that the introduction of positive charges leads to an increase in the activation energy, which might result from the Coulomb interaction between transporting electrons and positively charged molecules. It is worth noting that the bias-dependent activation energy of SMJ-1 drops from ≈70 meV to ≈20 meV when the bias voltage changes from 0.1 V to 1 V, while that of SMJ-2 fluctuates at 20 meV with a small drop at high bias voltages (Figures 2g–i). These results indicate that the positively charged systems show a greater dependence on bias voltage, for the reason that the charge transport process of the positively charged system is more sensitive to the bias voltage. The calculated activation energies of the transition states with adding an electron to the positively charged dimer (D1) and the neutral dimer (D2) are −0.78 eV and −0.19 eV (Figure S13), respectively. The larger activation energy leads to electron tunneling away from the sandwiched molecule as a rate-determining step. Therefore, the positively charged system is more sensitive to the bias voltage. In contrast, the activation energies of three SMJs at low temperatures are all less than 1 meV with no obvious bias-dependent features. Therefore, it is clear to conclude that in dimer systems, the transport transition is from temperature-independent coherent tunneling at low temperatures to thermally activated incoherent transport at high temperatures (Figure 3a).[24] In addition, positively charged units show a great ability to enhance the incoherent transport process.

The transition temperature from coherent to incoherent transport is a key parameter to understand the structure–property relationship of intermolecular charge transport mechanisms.[22a] Figure 3b shows the representative Arrhenius plots at 0.1 V, in which the extracted transition temperatures are about 92 K, 122 K, and 64 K for three SMJs based on positively charged (SMJ-1), neutral (SMJ-2), and weakly conjugated (SMJ-3) structures, respectively. From the bias-dependent analysis (Figure 3c), it is found that transition temperatures of the three SMJs have less dependence on the bias voltage. Specific molecular vibration modes are supposed to contribute to transport transition.[22] Apparent vibration peaks at 55 cm^{-1}, 87 cm^{-1} and 34 cm^{-1} for M1, M2, and M3, respectively, can be observed from the calculated vibration spectra (Figure 3e), which are related to the

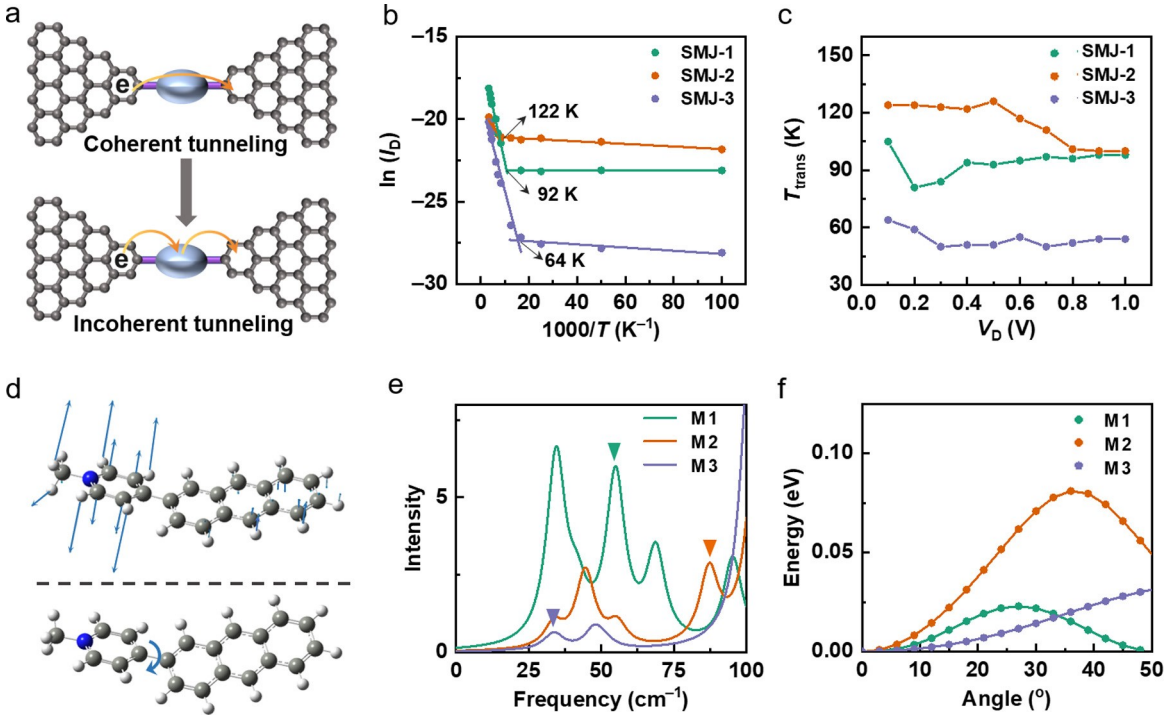

Figure 3. Mechanism for the charge transport transition. a) Schematic mechanism of the charge transport transition. b) Arrhenius plots of ln (I_D) versus 1/T at 0.1 V with marked transition temperatures. c) Transition temperatures of the charge transport transition under different bias voltages. d) Activated vibration modes (up) and rotation mode (bottom) of M1. e) Calculated vibration spectra of M1, M2, and M3. f) Potential energy as a function of rotation angle of the phenyl rings for M1, M2, and M3.

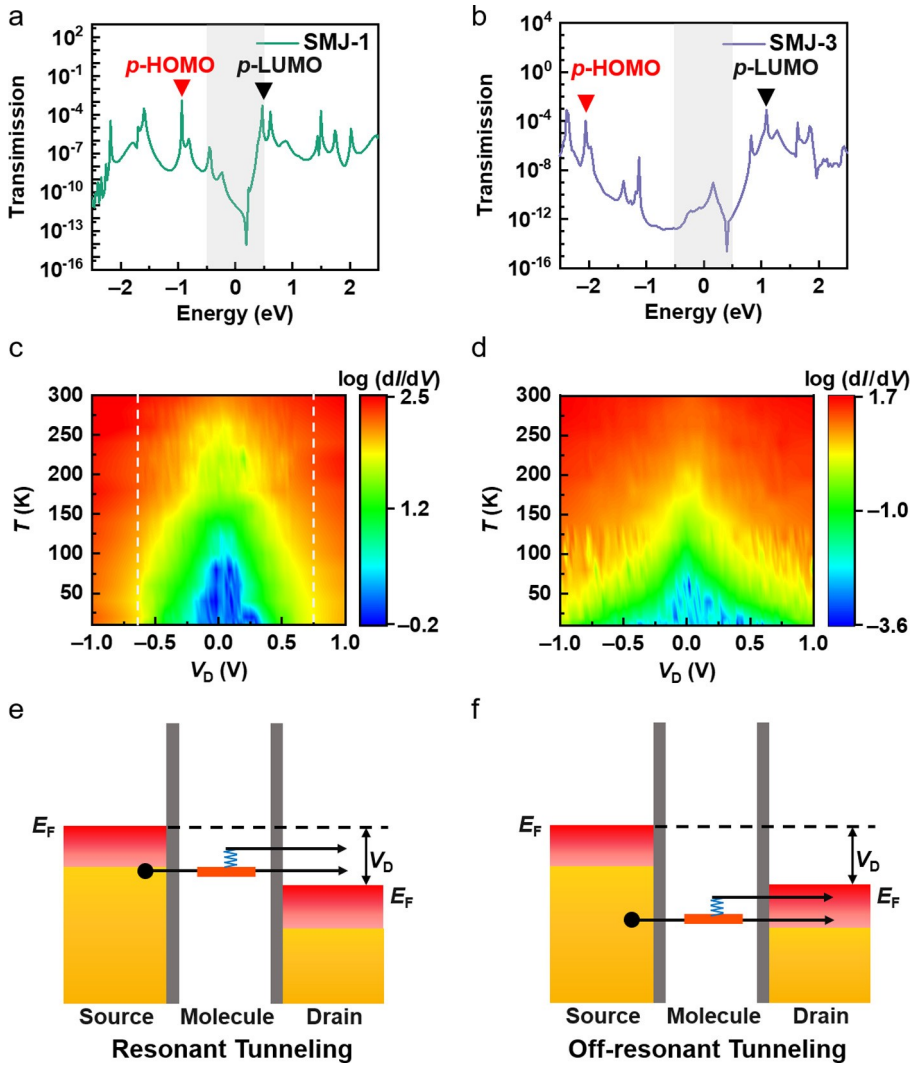

Figure 4. Energy level-dependent charge transport mechanism. Zero-bias voltage transmission spectra of a) SMJ-1, and b) SMJ-3. Gray shading shows the conductive window. The red and black triangles mark out the transmission peaks of *p*-HOMO and *p*-LUMO. Mapping of d*I*/d*V* versus V_D and *T* for c) SMJ-1, and d) SMJ-3. Dashed lines represent the division of resonant and off-resonant tunneling regions. Charge transport mechanism for e) resonant, and f) off-resonant tunneling. Red region represents the thermal-induced Fermi level broadening of the electrodes.

vibrational modes of aromatic rings (Figure 3d and Table S1). It is demonstrated that the calculated molecular vibrational energies are consistent with the thermal energies of the experimental transition temperatures (Table S2). Therefore, the incoherent transport mechanism involves thermally-induced vibration-assisted tunneling,[25] where thermal energy excites vibrations of molecules that couple with the transporting electrons. Notably, SMJ-3 shows the lowest transition temperature because the vibration mode between the phenyl rings occurs at low frequency in the weakly conjugated system. The transition temperature of SMJ-1 (80–105 K) is lower relative to that of SMJ-2 with a neutral system (100–126 K), which indicates that the positively charged unit is beneficial for phenyl vibrations with lower excitation energy. The reason could be that the delocalization degree for the positively charged M1 is enhanced due to the uneven distribution of electrostatic potential, which makes the vibration modes of the phenyl ring more easily excited with smaller thermal energy. From the view of the molecular rotation potential, at small rotation angles, the lowest potential of M3 indicates that the thermal energy at the low temperature enables to excite the rotation of pyridine ring (Figure 3f). Significantly, compared with M2, M1 exhibits a lower rotation potential of aromatic rings, which suggests that molecular rotation will lead to the transition of charge transport mechanism. In addition, the introduction of positive charge can reduce the rotation potentials, thus lowering the transition temperature of charge transport.

Energy level alignments play an essential role in regulating the charge transport mechanisms.[26] The differential conductance diagrams for SMJ-1 and SMJ-3 at 10 K show two distinct conductance regimes (Figure S14), i.e., region I (blue shading) with a conductance plateau and region II (yellow shading) with an increasing conductance, which indicates that the molecular orbitals enter into the

conductive window. Notably, the transition voltages for molecular orbitals entering the conductive window of SMJ-1 is about 0.33 V at positive voltages, which is smaller than that of SMJ-3 (about 0.78 V, Figure S14). According to the theoretical calculations, it is found that the perturbed lowest unoccupied molecular orbital (*p*-LUMO) of SMJ-1 and SMJ-3 presented in transmission spectra is close to the Fermi level, which reveals that *p*-LUMO is the main conductive channels for electron transport (Figures 4a and b). In addition, compared with SMJ-3, the *p*-LUMO of SMJ-1 with highly conjugated backbone is closer to the Fermi level (Figures S15–S17), indicating that a small bias voltage is sufficient for SMJ-1 to achieve resonant transport, which is consistent with experimental results.

Based on off-resonant and resonant charge transport, temperature-dependent charge transport mechanisms are further explored. From the temperature-dependent mapping of d*I*/d*V* versus V_D for SMJ-1 and SMJ-3 (Figures 4c and d), at the low bias region, corresponding to off-resonant tunneling, a continuous change of conductance with temperature is observed for both SMJs in the low temperature region (Figure S18). Since molecular vibration modes could not be excited at low temperatures, this temperature-dependent conductance change might be caused by thermally-induced Fermi level broadening. Specifically, the increased temperature leads to the molecular energy levels closer to the broadened Fermi level, thus contributing to the increase of molecular conductance.[27] For off-resonant tunneling in the high temperature region, the conductance of SMJ-1 and SMJ-3 enhances with the increase of temperature, which might be the result of the combined action of thermally induced vibron-assisted tunneling and the thermal broadening of the Fermi level of the electrode (Figure 4f). For resonant tunneling under high bias voltages, the temperature-dependent d*I*/d*V* spectra for highly conjugated SMJ-1 show a change in conductance at high temperatures because of the effect of thermally-assisted vibron-tunneling (Figure 4e). Nevertheless, at low temperatures, no apparent conductance increase of SMJ-1 is observed, indicating that the thermal broadening of the Fermi level has little effect.

Conclusion

A series of stable dimer single-molecule junctions with different charge states and energy levels have been constructed through supramolecular assembly using graphene-based static molecular junctions. A transition from temperature-independent coherent tunneling to temperature-dependent incoherent transport is observed, which is caused by thermally-induced specific molecular vibration modes. Significantly, the introduction of positive charge enables to enhance the incoherent transport with increased activation energy. Multiple thermal effects have been demonstrated to play a different role in regulating molecular conductance in off-resonant and resonant charge transport regions. Thermally-induced vibron-assisted tunneling play a partial role during the off-resonant transport and has a dominating impact on resonant transport. The in-depth understanding of the relationship between the molecular structures of dimers and the intermolecular charge transport at the single-molecule level provides fundamental guidance for development of desired functional organic materials and devices.

Acknowledgements

We acknowledge primary financial supports from the National Key R&D Program of China (2017YFA0204901, 2021YFA1200101, and 2021YFA1200102), the National Natural Science Foundation of China (22150013, 22173050, 21727806, and 21933001), the Tencent Foundation through the XPLORER PRIZE, "Frontiers Science Center for New Organic Matter" at Nankai University (63181206), the Fundamental Research Funds for the Central Universities (63223056), the Natural Science Foundation of Beijing (2222009), and Beijing National Laboratory for Molecular Sciences (BNLMS202105). The research carried out at Zhejiang University was supported by the Starry Night Science Fund of Zhejiang University Shanghai Institute for Advanced Study, Grant No. SN-ZJU-SIAS-006.

Conflict of Interest

The authors declare no conflict of interest.

Data Availability Statement

The data that support the findings of this study are available from the corresponding author upon reasonable request.

Keywords: Charge Transport · Dimer Junctions · Host–Guest Interaction · Intermolecular · Thermally-Induced Vibration

[1] a) K. Sato, R. Ichinoi, R. Mizukami, T. Serikawa, Y. Sasaki, J. Lutkenhaus, H. Nishide, K. Oyaizu, *J. Am. Chem. Soc.* **2018**, *140*, 1049–1056; b) Y. Tan, N. C. Casetti, B. W. Boudouris, B. M. Savoie, *J. Am. Chem. Soc.* **2021**, *143*, 11994–12002.

[2] a) L. J. C. Jeuken, A. K. Jones, S. K. Chapman, G. Cecchini, F. A. Armstrong, *J. Am. Chem. Soc.* **2002**, *124*, 5702–5713; b) A. R. Arnold, M. A. Grodick, J. K. Barton, *Cell Chem. Biol.* **2016**, *23*, 183–197.

[3] a) V. Coropceanu, J. Cornil, D. A. da Silva Filho, Y. Olivier, R. Silbey, J.-L. Brédas, *Chem. Rev.* **2007**, *107*, 926–952; b) G. Gryn′ova, C. Corminboeuf, *J. Phys. Chem. Lett.* **2018**, *9*, 2298–2304.

[4] a) C. Wang, H. Dong, W. Hu, Y. Liu, D. Zhu, *Chem. Rev.* **2012**, *112*, 2208–2267; b) M. Muccini, *Nat. Mater.* **2006**, *5*, 605–613.

[5] G. Hong, X. Gan, C. Leonhardt, Z. Zhang, J. Seibert, J. M. Busch, S. Bräse, *Adv. Mater.* **2021**, *33*, 2005630.

[6] O. Ostroverkhova, *Chem. Rev.* **2016**, *116*, 13279–13412.

[7] Y. Zhao, L. Liu, F. Zhang, C. Di, D. Zhu, *SmartMat* **2021**, *2*, 426–445.

[8] a) C. Wang, H. Dong, L. Jiang, W. Hu, *Chem. Soc. Rev.* **2018**, *47*, 422–500; b) S. Fratini, M. Nikolka, A. Salleo, G. Schweicher, H. Sirringhaus, *Nat. Mater.* **2020**, *19*, 491–502; c) G. R.

Hutchison, M. A. Ratner, T. J. Marks, *J. Am. Chem. Soc.* **2005**, *127*, 16866–16881.
[9] a) C. Joachim, A. Ratner Mark, *Proc. Natl. Acad. Sci. USA* **2005**, *102*, 8801–8808; b) A. Batra, G. Kladnik, H. Vazquez, J. S. Meisner, L. Floreano, C. Nuckolls, D. Cvetko, A. Morgante, L. Venkataraman, *Nat. Commun.* **2012**, *3*, 1086; c) S. V. Aradhya, L. Venkataraman, *Nat. Nanotechnol.* **2013**, *8*, 399–410; d) Q. Li, G. C. Solomon, *Faraday Discuss.* **2014**, *174*, 21–35; e) S. Fujii, T. Tada, Y. Komoto, T. Osuga, T. Murase, M. Fujita, M. Kiguchi, *J. Am. Chem. Soc.* **2015**, *137*, 5939–5947; f) H. Chen, H. Zheng, C. Hu, K. Cai, Y. Jiao, L. Zhang, F. Jiang, I. Roy, Y. Qiu, D. Shen, Y. Feng, F. M. Alsubaie, H. Guo, W. Hong, J. F. Stoddart, *Matter* **2020**, *2*, 378–389.
[10] a) S. T. Schneebeli, M. Kamenetska, Z. Cheng, R. Skouta, R. A. Friesner, L. Venkataraman, R. Breslow, *J. Am. Chem. Soc.* **2011**, *133*, 2136–2139; b) A. Magyarkuti, O. Adak, A. Halbritter, L. Venkataraman, *Nanoscale* **2018**, *10*, 3362–3368; c) S. Wu, M. T. González, R. Huber, S. Grunder, M. Mayor, C. Schönenberger, M. Calame, *Nat. Nanotechnol.* **2008**, *3*, 569–574.
[11] a) T. Fu, S. Smith, M. Camarasa-Gómez, X. Yu, J. Xue, C. Nuckolls, F. Evers, L. Venkataraman, S. Wei, *Chem. Sci.* **2019**, *10*, 9998–10002; b) Y. Zhao, W. Liu, J. Zhao, Y. Wang, J. Zheng, J. Liu, W. Hong, Z.-Q. Tian, *Int. J. Extrem. Manuf.* **2022**, *4*, 022003.
[12] a) S. Martín, I. Grace, M. R. Bryce, C. Wang, R. Jitchati, A. S. Batsanov, S. J. Higgins, C. J. Lambert, R. J. Nichols, *J. Am. Chem. Soc.* **2010**, *132*, 9157–9164; b) R. Frisenda, V. A. E. C. Janssen, F. C. Grozema, H. S. J. van der Zant, N. Renaud, *Nat. Chem.* **2016**, *8*, 1099–1104; c) S. Caneva, P. Gehring, V. M. García-Suárez, A. García-Fuente, D. Stefani, I. J. Olavarria-Contreras, J. Ferrer, C. Dekker, H. S. J. van der Zant, *Nat. Nanotechnol.* **2018**, *13*, 1126–1131.
[13] X. Chen, M. Roemer, L. Yuan, W. Du, D. Thompson, E. del Barco, C. A. Nijhuis, *Nat. Nanotechnol.* **2017**, *12*, 797–803.
[14] a) N. J. Kay, S. J. Higgins, J. O. Jeppesen, E. Leary, J. Lycoops, J. Ulstrup, R. J. Nichols, *J. Am. Chem. Soc.* **2012**, *134*, 16817–16826; b) J. Bai, X. Li, Z. Zhu, Y. Zheng, W. Hong, *Adv. Mater.* **2021**, *33*, 2005883.
[15] W. Haiss, H. van Zalinge, S. J. Higgins, D. Bethell, H. Höbenreich, D. J. Schiffrin, R. J. Nichols, *J. Am. Chem. Soc.* **2003**, *125*, 15294–15295.
[16] a) H. Chen, J. Fraser Stoddart, *Nat. Rev. Mater.* **2021**, *6*, 804–828; b) S. Li, J. Li, H. Yu, S. Pudar, B. Li, J. Rodríguez-López, J. S. Moore, C. M. Schroeder, *J. Electroanal. Chem.* **2020**, *875*, 114070; c) D. C. Milan, M. Krempe, A. K. Ismael, L. D. Movsisyan, M. Franz, I. Grace, R. J. Brooke, W. Schwarzacher, S. J. Higgins, H. L. Anderson, C. J. Lambert, R. R. Tykwinski, R. J. Nichols, *Nanoscale* **2017**, *9*, 355–361; d) H. Yu, J. Li, S. Li, Y. Liu, N. E. Jackson, J. S. Moore, C. M. Schroeder, *J. Am. Chem. Soc.* **2022**, *144*, 3162–3173.
[17] W. Zhang, S. Gan, A. Vezzoli, R. J. Davidson, D. C. Milan, K. V. Luzyanin, S. J. Higgins, R. J. Nichols, A. Beeby, P. J. Low, B. Li, L. Niu, *ACS Nano* **2016**, *10*, 5212–5220.
[18] C. Jia, B. Ma, N. Xin, X. Guo, *Acc. Chem. Res.* **2015**, *48*, 2565–2575.
[19] S. J. Barrow, S. Kasera, M. J. Rowland, J. del Barrio, O. A. Scherman, *Chem. Rev.* **2015**, *115*, 12320–12406.
[20] a) Y. Cao, S. Dong, S. Liu, L. He, L. Gan, X. Yu, M. L. Steigerwald, X. Wu, Z. Liu, X. Guo, *Angew. Chem. Int. Ed.* **2012**, *51*, 12228–12232; *Angew. Chem.* **2012**, *124*, 12394–12398; b) Y. Cao, S. Dong, S. Liu, Z. Liu, X. Guo, *Angew. Chem. Int. Ed.* **2013**, *52*, 3906–3910; *Angew. Chem.* **2013**, *125*, 3998–4002.
[21] C. Jia, A. Migliore, N. Xin, S. Huang, J. Wang, Q. Yang, S. Wang, H. Chen, D. Wang, B. Feng, Z. Liu, G. Zhang, D.-H. Qu, H. Tian, M. A. Ratner, H. Q. Xu, A. Nitzan, X. Guo, *Science* **2016**, *352*, 1443–1445.
[22] a) Y. Selzer, M. A. Cabassi, T. S. Mayer, D. L. Allara, *J. Am. Chem. Soc.* **2004**, *126*, 4052–4053; b) N. Xin, C. Jia, J. Wang, S. Wang, M. Li, Y. Gong, G. Zhang, D. Zhu, X. Guo, *J. Phys. Chem. Lett.* **2017**, *8*, 2849–2854.
[23] D. Segal, A. Nitzan, M. Ratner, W. B. Davis, *J. Phys. Chem. B* **2000**, *104*, 2790–2793.
[24] T. Hines, I. Diez-Perez, J. Hihath, H. Liu, Z.-S. Wang, J. Zhao, G. Zhou, K. Müllen, N. Tao, *J. Am. Chem. Soc.* **2010**, *132*, 11658–11664.
[25] P. Li, L. Zhou, C. Zhao, H. Ju, Q. Gao, W. Si, L. Cheng, J. Hao, M. Li, Y. Chen, C. Jia, X. Guo, *Rep. Prog. Phys.* **2022**, *85*, 086401.
[26] C. Jia, X. Guo, *Chem. Soc. Rev.* **2013**, *42*, 5642–5660.
[27] a) M. Kondratenko, S. R. Stoyanov, S. Gusarov, A. Kovalenko, R. L. McCreery, *J. Phys. Chem. C* **2015**, *119*, 11286–11295; b) A. J. Bergren, R. L. McCreery, S. R. Stoyanov, S. Gusarov, A. Kovalenko, *J. Phys. Chem. C* **2010**, *114*, 15806–15815.

Manuscript received: July 25, 2022
Accepted manuscript online: September 13, 2022
Version of record online: October 6, 2022